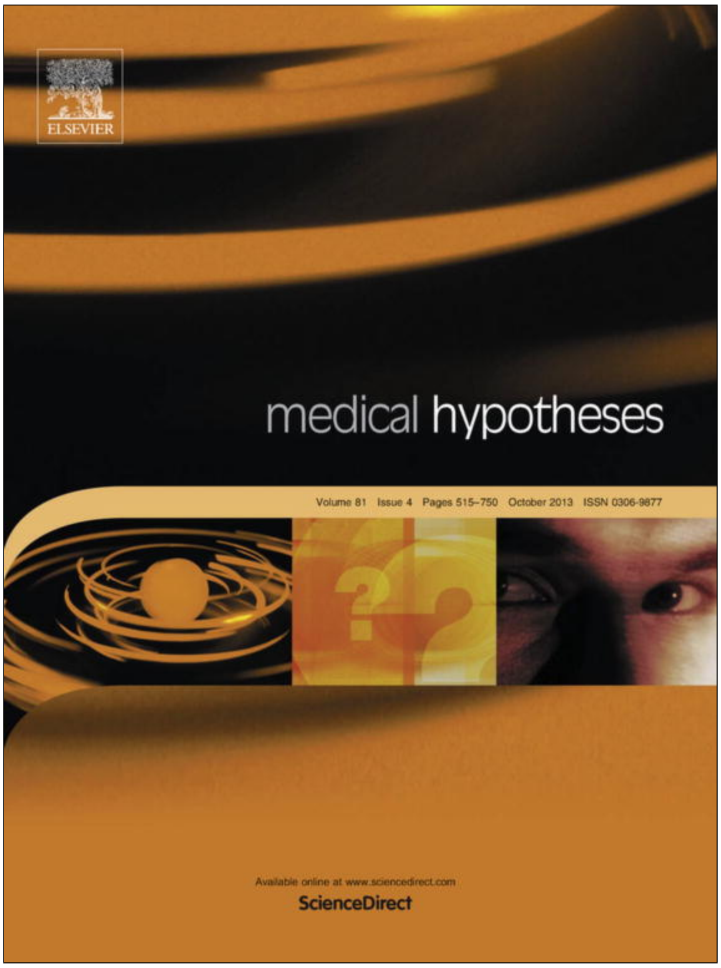
ELSEVIER
medical hypotheses
Volume 81 Issue 4 Pages 515–750 October 2013 ISSN 0306-9877
Available online at www.sciencedirect.com
ScienceDirect

Medical Hypotheses 81 (2013) 738–744

Contents lists available at ScienceDirect

Medical Hypotheses

journal homepage: www.elsevier.com/locate/mehy

Three-dimensional kinematic stress magnetic resonance image analysis shows promise for detecting altered anatomical relationships of tissues in the cervical spine associated with painful radiculopathy

N.V. Jaumard [a,b], J.K. Udupa [c], S. Siegler [e], J.M. Schuster [b], A.S. Hilibrand [d], B.E. Hirsch [f], A. Borthakur [c], B.A. Winkelstein [a,b,*]

[a] Department of Bioengineering, University of Pennsylvania, Philadelphia, PA, United States
[b] Department of Neurosurgery, University of Pennsylvania, Philadelphia, PA, United States
[c] Department of Radiology, University of Pennsylvania, Philadelphia, PA, United States
[d] Department of Orthopaedic Surgery, Jefferson Medical College, Rothman Institute, Philadelphia, PA, United States
[e] Mechanical Engineering & Mechanics, Drexel University, Philadelphia, PA, United States
[f] Neurobiology & Anatomy, Drexel University, Philadelphia, PA, United States

ARTICLE INFO

Article history:
Received 8 May 2013
Accepted 20 July 2013

ABSTRACT

For some patients with radiculopathy a source of nerve root compression cannot be identified despite positive electromyography (EMG) evidence. This discrepancy hampers the effective clinical management for these individuals. Although it has been well-established that tissues in the cervical spine move in a three-dimensional (3D) manner, the 3D motions of the neural elements and their relationship to the bones surrounding them are largely unknown even for asymptomatic normal subjects. We hypothesize that abnormal mechanical loading of cervical nerve roots during pain-provoking head positioning may be responsible for radicular pain in those cases in which there is no evidence of nerve root compression on conventional cervical magnetic resonance imaging (MRI) with the neck in the neutral position. This biomechanical imaging proof-of-concept study focused on quantitatively defining the architectural relationships between the neural and bony structures in the cervical spine using measurements derived from 3D MR images acquired in neutral and pain-provoking neck positions for subjects: (1) with radicular symptoms and evidence of root compression by conventional MRI and positive EMG, (2) with radicular symptoms and no evidence of root compression by MRI but positive EMG, and (3) asymptomatic age-matched controls. Function and pain scores were measured, along with neck range of motion, for all subjects. MR imaging was performed in both a neutral position and a pain-provoking position. Anatomical architectural data derived from analysis of the 3D MR images were compared between symptomatic and asymptomatic groups, and the symptomatic groups with and without imaging evidence of root compression. Several differences in the architectural relationships between the bone and neural tissues were identified between the asymptomatic and symptomatic groups. In addition, changes in architectural relationships were also detected between the symptomatic groups with and without imaging evidence of nerve root compression. As demonstrated in the data and a case study the 3D stress MR imaging approach provides utility to identify biomechanical relationships between hard and soft tissues that are otherwise undetected by standard clinical imaging methods. This technique offers a promising approach to detect the source of radiculopathy to inform clinical management for this pathology.

Introduction

Making a definitive diagnosis that can direct further treatment is a major difficulty in treating spinal disorders. For most people with pain in the neck and low back and radiating to the limbs, a specific source or "pain generator" cannot be identified using conventional, or even sophisticated, imaging techniques. These patients may experience long-term disability, resulting in high medical costs and imposing major indirect costs to society in terms of lost productivity. Cervical radiculopathy is a common source of chronic pain with symptoms that can persist for long periods of time. In many instances, mechanical factors in the spine, including joint dysfunction, disc herniation or protrusion, foraminal occlusion, and abnormal vertebral motions, can contribute to painful cervical nerve root loading [1–4]. However, due to the sometimes

* Corresponding author. Address: Department of Bioengineering, University of Pennsylvania, 240 Skirkanich Hall, 210 S 33rd St., Philadelphia, PA 19104-6321, United States. Tel.: +1 215 573 4589; fax: +1 215 573 2071.

E-mail address: winkelst@seas.upenn.edu (B.A. Winkelstein).

0306-9877/$ - see front matter © 2013 Elsevier Ltd. All rights reserved.
http://dx.doi.org/10.1016/j.mehy.2013.07.043

transient, and typically complicated, architectural relationships between the tissues of the spine, it is not always possible to detect changes in local tissue loading.

Although disc herniation and foraminal stenosis may be identified by traditional static imaging approaches, such as magnetic resonance imaging (MRI) and computed tomography (CT)-myelography, many patients present with pain symptoms but lack definitive imaging evidence of compression of the nerve roots or the spinal cord [5]. Furthermore, static imaging cannot identify a specific symptomatic site when nerve root compression affects several spinal levels. In addition, radiculopathy can be caused by transient nerve compression due to altered motion associated with arthritic changes. In the neck, the potential for loading of the nerve roots (either by radial compression or axial tension) due to head and torso motions is high given the extreme flexibility and coupled rotations of the cervical spine [6–9]. Cervical nerve root pinching has been attributed to foraminal narrowing in as many as 93% of radiculopathy cases [10,11]. In fact, the foraminal space available for the nerve root can decrease by up to 20% for movements within normal neck bending motions [4] and is even greater for the cases of trauma and the arthritic spine [3]. Although these studies support mechanical irritation to the nerve root as contributing to radicular pain in the cervical spine, they do not differentiate static from dynamic mechanisms of such loading, nor are they able to evaluate the possibility that altered loading to the nerve roots or nerves may occur along the spinal column and in a variety of directions. Without information on the normal and abnormal neural tissue biomechanics, current diagnostic capabilities are limited only to the identification of visible tissue compression in the static condition.

Several types of imaging procedures have been employed to study cervical spine disorders. Radiographs have been used to quantify linear and angular intervertebral motions either in the intact condition or after damage to posterior cervical structures, and to understand injury mechanisms [12–14]. They also have been used in conjunction with MRI to focus only on soft tissue damage (such as disc herniation) by excluding hard tissue abnormalities such as osteophytes [15]. Multi-slice MRI is the most common approach used to define anatomical changes and infer tissue biomechanics in the cervical spine. However, such approaches are limited to two-dimensional (2D) measurements for imaging of the vertebrae in the neutral position for non-weight bearing situations only [16–18]. Despite the known three-dimensional (3D) coupling in the spine, the more-complicated out-of-plane loading scenarios, such as lateral bending and axial torsion, are infrequently and inadequately studied using 2D approaches [19–24]. Although 3D MRI sequences can distinguish tissue boundaries to provide better slice profiles and improved sensitivity [25], there has been very limited application of 3D analysis techniques for either MRI or CT in the spine. Further, the focus of these 3D imaging approaches has been mostly on defining the relative movement of the vertebrae [21,26–28], and the identification of anatomic anomalies, such as the location of disc herniation and foraminal compromise, have remained qualitative [16].

A recently developed imaging method known as '3D stress MRI' (3D sMRI) has been successfully used to study the kinematics and mechanics of joints with complicated articulations in the foot and ankle [29–31]. These analyses have shown the ability of sMRI to distinguish between normal joints and joints with some abnormality, such as architectural distortions of the foot or ligament injury, in terms of the 3D architecture of the bones and their kinematics. Although 3D MRI and CT analysis techniques have been used to define the 3D kinematics of cervical vertebrae during physiologic bending and torsion [21,26–28,32], the 3D motions of the neural elements (i.e. spinal cord, nerve roots, and spinal nerves) and their relationship to the bones surrounding them are largely unknown even for asymptomatic normal subjects.

Based on the biomechanics of the cervical spine and 3D sMRI exhibiting the ability to discriminate between normal and abnormal architecture and kinematics in other joints, we hypothesize that 3D stress MRI can be used to evaluate the 3D motion of both bony and neural elements of the cervical spine. It is further hypothesized that abnormal nerve root mechanical loading (as indicated by altered architectural relationships between bones and neural tissue) during pain-provoking head/neck positioning can be detected in patients who demonstrate radiculopathy symptoms. Specifically, we tested the hypothesis that anatomical signs of radiculopathy that are not detectable using conventional planar imaging may be related to abnormal nerve root and spinal cord loading that is caused by altered nerve-bone architectural relationships in the cervical spine. We used 3D stress MRI to measure several relevant anatomical relationships in both symptomatic and asymptomatic populations and to demonstrate the potential utility of this approach for clinical assessment of otherwise unidentifiable spinal pathologies. Comparisons of the architectural measurements between the symptomatic and asymptomatic populations were performed to identify potential patterns of differences relating to the differences in pain levels. Further, a case study is also presented to illustrate the clinical utility of the 3D sMRI method in identifying a potential source of nerve root compression that was not detected using traditional imaging.

Methods

The objective of this study was to characterize the architectural relationships between neural and bony structures in the cervical spine using measurements derived from 3D stress MRI for both neutral and pain-provoking neck positions, as well as the changes between those two positions. All procedures were approved by the Institutional Review Board and adhered to the guidelines of the Committee for Research and Ethical Issues of the International Association for the Study of Pain. Subjects with cervical radicular pain evoked by head movements, both with and without evidence of nerve root compression on clinical imaging, were included in this pilot study. In addition, age-matched asymptomatic subjects were also included to provide a control group in which changes in architectural parameters are not related to the onset of pain.

For this study, function and pain were assessed for all subjects at baseline before MR imaging, using range of motion (ROM), the Neck Disability Index (NDI), and the Verbal Rating Score (VRS) [33]. Each symptomatic subject underwent MR scans in neutral and a pain-provoking position; the VRS was again assessed after scanning in each of the neutral and pain-provoking positions. Architectural data from analysis of the 3D sMRI were examined and compared between the symptomatic and asymptomatic groups, and between the symptomatic groups with and without imaging evidence of nerve root compression, to evaluate the ability of this imaging technique to detect any differences in the relationships between the tissues in the cervical spine.

Function and pain assessment

Symptomatic subjects ($n = 10$) with a diagnosis of cervical radiculopathy based on positive findings on EMG and pain radiating down one or both arms were included in this feasibility study. Of those, a subgroup ($n = 5$) exhibited evidence of nerve root compression based on conventional clinical radiological imaging, while the other subgroup ($n = 5$) had no such imaging evidence. NDI and VRS scores for arm and neck pain were recorded at the start of each session (baseline). Neck range of motion (ROM) was also measured in flexion–extension, left and right lateral bending, and left and right axial torsion using a CROM goniometer device (Performance

Attainment Associates; Lindstrom, MN) at baseline. In addition, the symptomatic subjects were asked to place their head in the position that evoked their radicular pain and the direction and angle(s) of that position were also measured using the CROM. After each of the scans the subjects were again interviewed to provide a VRS score for their arm and neck pain. The NDI, VRS and ROM data at baseline were compared between symptomatic and asymptomatic groups using a *t*-test with significance at $p < 0.05$. The VRS scores after the neutral and pain-provoking scans were also compared between the two groups. In addition, the VRS scores after each scan were separately compared to baseline for each position, using a paired *t*-test.

MR imaging

Asymptomatic ($n = 10$; 36.9 ± 14.7 years; 7M, 3F) and symptomatic ($n = 8$; 49.6 ± 11.0 years; 4M, 6F) subjects underwent MRI of the cervical spine (from C2-C7) using a Siemens 3T Tim Trio scanner (Siemens Medical Solutions, Malvern, PA). Extensive pilot studies were performed which led to two separate sMRI acquisition protocols to optimally define the bone and neural tissues. The bone protocol used a FLASH 3D pulse sequence with an image matrix size of 512×512, a voxel size of $0.3 \times 0.3 \times 1$ mm^3, and a TE/TR = 4 ms/9 ms to acquire 120 slices in the sagittal plane in 7 min. The neural tissue protocol used a 320×320 matrix size, a voxel size of $0.5 \times 0.5 \times 0.8$ mm^3, and TE/TR = 137 ms/1610 ms to acquire 120 slices in the axial plane in 10 min. Slicing in the sagittal and axial planes, respectively, minimized partial volume effects and the subsequent blurring of the vertebral and nerve root boundaries. The two protocols were performed in each of the neutral and pain-provoking (stressed) positions for the symptomatic subjects. For the asymptomatic subjects, the two scanning protocols were performed in the neutral position, as well as in left and right axial torsion.

Image analysis

The acquired images were processed with 3DVIEWNIX software to derive metrics describing the 3D architectural relationship among the spinal cord, nerve roots, and the vertebrae [34]. To reduce artifacts caused by non-uniformity and non-repeatability of the image intensity, the images were rectified using previously described methods [35,36]. To reduce the bias caused by the discrepancy between acquisition planes for different subjects and by intra-subject motion between the sagittal and axial image acquisitions, all images were registered within a common coordinate system. This registration operation was performed assuming a rigid transformation and by maximizing the mutual information between the two images [37]. The bone image was then transformed to match with the neural tissue image and was subsequently resliced in the axial plane. In this manner, both the bone and neural tissue information were portrayed in a single display of this registered image pair (Fig. 1).

The vertebrae, spinal cord, and nerve roots were delineated using the registered and rectified images, according to optimal methods for each tissue type. Bone was delineated in the sagittal bone images using the semi-automatic live wire method [38] for slice-by-slice demarcation of the boundaries of the vertebrae. The spinal cord was segmented in the axial neural tissue images by a more automated method called 'fuzzy connectedness' [39]. The nerve roots were also delineated in the axial neural tissue images; although the nerve roots are well-visualized in the subarachnoid space filled with cerebrospinal fluid (CSF), they become progressively more difficult to locate as they combine and proceed peripherally towards the foraminal space. Because of this difficulty, a region including the CSF space was first manually outlined within each slice, and within the 3D space defined by these regions, the neural tissue was segmented by fuzzy thresholding via a trapezoidal function [33].

Distances and angles defining the 3D architectural relationship between the nerve roots, spinal cord, and the vertebrae were measured at each of the five cervical levels (C2-C3 through C6-C7) for each subject with the neck in each position (Fig. 2). Fused images with bone and neural tissues having optimal visualization resulted from the image registration and were used to identify tissue-specific points for all measurements. The angulation of the bilateral dorsal and ventral nerve roots from the point they emanate from the spinal cord to where they exit through the neural foramen,

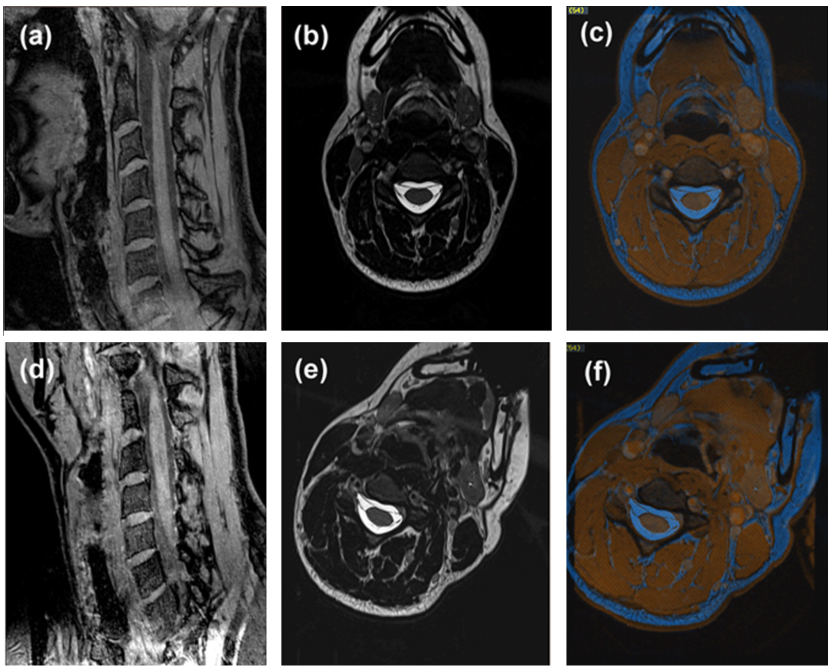

Fig. 1. Slice images for one subject showing the bone and neural images (a, b, d, and e), as well as the registered bone and nerve root images (c and f). The top row (a–c) shows the images corresponding to neutral and the bottom row (d–f) corresponds to left torsion of the head.

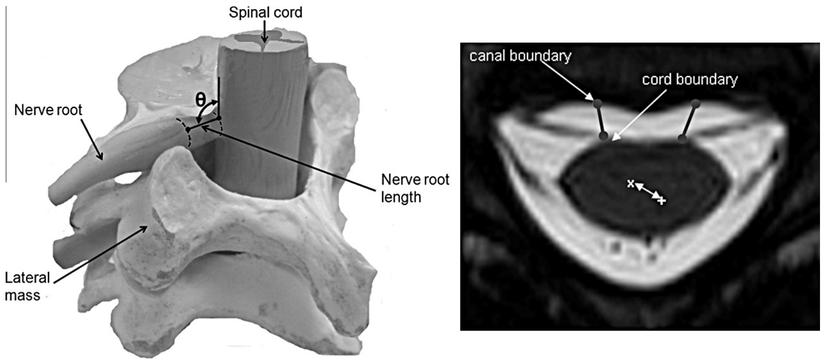

Fig. 2. Schematic indicating measurements made at each cervical level from the stress MRI: both the nerve root angulation (θ) and length are shown on the left. On the right, the canal and spinal cord boundaries are indicated on the axial image, as well as the center of the cord (x) and the center of the canal (+). The distance between those (indicated by double arrow) is the offset and the cord-to-canal measurements (indicated by line segments) are shown on the right and left.

Table 1
Summary of pain, function and ROM (in degrees) at baseline for both subject groups.

	Asymptomatic	Symptomatic	Significant
NDI	0.6 ± 0.1	40.1 ± 16.5	$p < 0.0001$
VRS – neck	0.1 ± 0.3	3.8 ± 2.8	$p = 0.002$
VRS – arm	0.0 ± 0.0	2.1 ± 2.7	$p = 0.038$
ROM			
Flexion	63.5 ± 12.1	48.3 ± 14.8	$p = 0.022$
Extension	70.4 ± 15.2	47.6 ± 11.8	$p = 0.002$
Right LB	49.1 ± 18.2	36.6 ± 11.9	
Left LB	51.5 ± 10.9	41.7 ± 12.6	
Right torsion	71.0 ± 9.1	58.9 ± 18.3	
Left torsion	64.6 ± 10.1	55.1 ± 15.2	

with respect to the central axis of the spinal cord, were specified (Fig. 2). Nerve root length was measured as the length of the line segment from the point of emanation of each root from the spinal cord to its point of exit at the foramen. Lastly, the relationship of the cord-to-canal at each slice level (one per vertebra) passing through the geometric center of the 3D vertebra was described by three measurements: (1) the offset between the centers of the spinal cord and the canal, and (2 & 3) the distance between the spinal cord and canal boundaries on each of the right and left sides (Fig. 2). The measurements in the neutral and pain-provoking positions were compared between the asymptomatic and symptomatic groups. Also, the change in measurements from neutral to the stressed pain-provoking position between the symptomatic groups and the asymptomatic group were compared. Both of these types of comparisons were also made between the two symptomatic groups. Although the group sizes are recognized as small, statistical comparisons were performed using t-tests with significance at $p < 0.05$ in order to assess if this technique may prove to be feasible for detecting changes in architectural relationships from asymptomatic conditions.

Repeatability analysis

To analyze the precision of these imaging and image analysis methods in making measurements, three of the asymptomatic subjects underwent the entire imaging process two times. After the first session of scanning, they were removed from and repositioned in the scanner for a second acquisition of imaging in the neutral and stressed neck positions. All processing and analysis procedures described above were performed on these datasets and the variations in the measurements between the two scan sessions were computed.

Results

The baseline NDI score was significantly different ($p < 0.0001$) between the asymptomatic (0.6 ± 1.0%) and symptomatic (40.1 ± 16.6%) subjects (Table 1). For all of the symptomatic subjects except one, a head position of axial torsion (either to the right or left) was the position reported to provoke their pain. In one subject a 30° extension of the head was reported as the pain-provoking position. The average torsion angle associated with pain provocation in the remaining subjects was 36.7 ± 13.9°. The ROM in all directions was lower for symptomatic compared to asymptomatic subjects (Table 1). However, the only significant differences in ROM between the groups were in flexion ($p = 0.022$) and extension ($p = 0.002$) (Table 1).

The VRS scores for neck and arm pain at baseline were both significantly higher (neck $p = 0.002$; arm $p = 0.038$) for symptomatic subjects (neck 3.8 ± 2.8; arm 2.1 ± 2.7) than for asymptomatic subjects (neck 0.1 ± 0.3; arm 0.0 ± 0.0) (Table 1; Fig. 3). After the neutral scan, ratings for neck and arm pain remained significantly higher (neck $p = 0.004$; arm $p = 0.003$) for symptomatic (neck 3.2 ± 2.5; arm 3.3 ± 2.6) than for asymptomatic (neck & arm 0.1 ± 0.3) subjects, and were not different from their corresponding baseline values for either group (Fig. 3). However, after the scan in the pain-provoking position, the VRS rating of arm pain (4.8 ± 3.2) increased significantly ($p = 0.022$) for the symptomatic group but

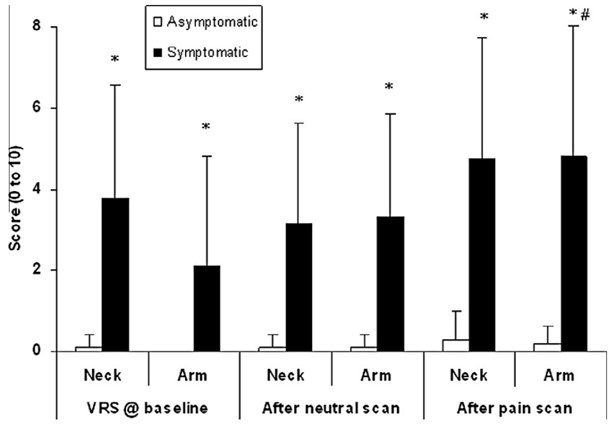

Fig. 3. VRS ratings for neck and arm pain at baseline, after the neutral scan, and after the pain-provoking scans for asymptomatic and symptomatic subjects. The VRS scores rating neck and arm pain for the symptomatic subjects were significantly greater (*) than those for the asymptomatic subjects for all evaluation times. After the pain-provoking scan, the arm pain VRS score was increased significantly (#) over baseline values for the symptomatic group.

Table 2
Summary of significant comparisons in the architectural differences between groups.

Asymptomatic vs. symptomatic without evidence
(1) Cord-to canal distance (right) in neutral at C3-4, C5-6; $p \leqslant 0.05$
(2) Cord-to-canal distance (left) in torsion at C5-6-7; $p \leqslant 0.04$
(3) Dorsal root length (right) in neutral at C6-7; $p = 0.05$
Asymptomatic vs. symptomatic with evidence
(1) Change in ventral root length (right) at C4-5; $p = 0.01$
(2) Change in cord-to-canal offset at C6-7; $p = 0.03$
(3) Change in cord-to-canal distance at C3-4; $p = 0.04$
Symptomatic without vs. with evidence
(1) Cord-to canal distance in neutral at C2-3-4; $p < 0.05$
(2) Change in cord-to-canal distance in torsion at C2-3-4; $p \leqslant 0.05$
(3) Change in ventral root length in torsion at C4-5; $p \leqslant 0.05$

the neck rating (4.8 ± 3.0) was not increased further by the pain-positioning (Fig. 3). However, the VRS scores for both neck and arm pain after the pain-provoking scan were significantly greater (neck $p = 0.001$; arm $p = 0.001$) than the corresponding scores for the asymptomatic group (neck 0.3 ± 0.7; arm 0.2 ± 0.4) after undergoing a scan with their head in axial torsion (Fig. 3). The VRS rating of arm pain in torsion was also significantly greater after the pain-provoking than after the neutral scan ($p = 0.005$) in the symptomatic group.

Complete analysis of the cervical spine scans was performed on all of the asymptomatic subjects, but was only possible for eight of the symptomatic subjects, owing to the fact that the neck did not remain stationary during the scanning in those subjects. In those two cases, the subject did not maintain a stationary position during one or several of the scans resulting from either anxiety medication causing heavy sedation and deep breathing or sudden movement during the MR imaging. The average percent coefficients of variation in the measurements between two repeated scans in each position for the three asymptomatic subjects were 3.1% for nerve root angulation, 1.2% for nerve root length, and 7.3% for the cord-to-canal measurements.

A total of 60 measurements and 150 related calculations (changes) were performed using the MR images. No particular pattern of differences was identified when comparing the architectural measurements and changes of each symptomatic group to those of the asymptomatic group. However, a few significant differences in the architectural measurements were detected between the asymptomatic and symptomatic groups, and between the two symptomatic groups (Table 2). In particular, the cord-to-canal measurements exhibited the most common significant differences. Interestingly, nerve root measurements were not commonly identified as being sensitive architectural metrics in the symptomatic group, regardless of whether there was or was not imaging evidence of nerve root compression. Significant differences were identified when comparing the symptomatic group without imaging evidence to that with imaging evidence (Table 2), and they were localized in the upper and middle cervical spines.

Case study

Interestingly, one of the patients in the symptomatic group (female, age 39 years) that had no evidence of tissue compression by conventional clinical imaging did demonstrate evidence of compression of the spinal cord and neural tissue in the images that were obtained using the stress MRI protocol (Fig. 4). That imaging protocol performed in the pain-provoking position was able to demonstrate a right-sided foraminal stenosis (C5 nerve root) and

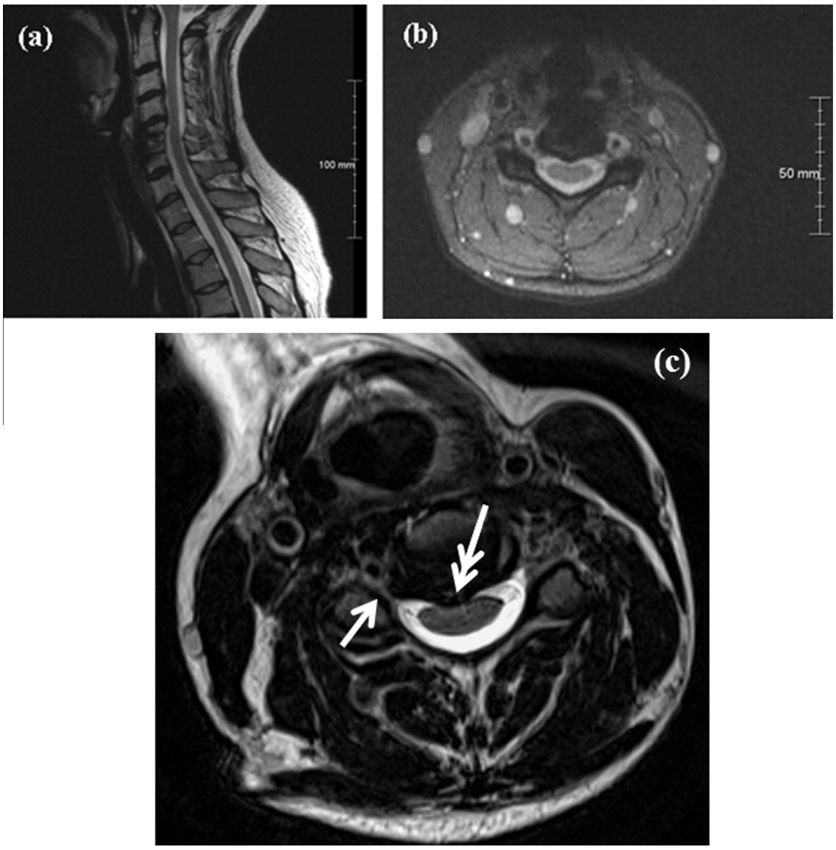

Fig. 4. MR images of a symptomatic patient presenting with EMG signs suggesting C5 radiculopathy. Sagittal (a) and axial (b) clinical MR images are unremarkable. However, compression of the right nerve root (arrow) and spinal cord (double arrow) are clearly visible on an axial stress MR image (c) taken with the head in the pain-provoking position.

a midline spinal cord compression by a herniated disc that were clearly identified on the images taken with the head in right axial rotation (Fig. 4). This finding further supports the hypothesis that abnormal neural tissue loading during pain-provoking positioning may be detected in patients who demonstrate radiculopathy symptoms but lack evidence on conventional planar or neutral imaging studies.

Discussion

It has been suggested that patients who do not have evidence of discrete nerve root compression on conventional static imaging may be affected by a transient dynamic compressive pathology. Such a phenomenon may involve both compression and irritation of the exiting nerve root produced during head and/or neck movements such as flexion, extension, and axial rotation [40]. Clinicians have conjectured that many of the subtle sources of dynamic nerve root compression may require multi-dimensional detection using an active imaging modality that accommodates a non-neutral reference of the spine. For example, many patients exhibit cervical radiculopathy only as a result of specific neck positioning. The clinician can reproduce this position and the associated symptoms through physical examination including performance of Spurling's maneuver or production of Lhermitte's phenomenon [40,41]. Coupling such physical examination maneuvers with an adequate imaging method could help to identify if, and how, the architectural relationship between the hard and soft tissues of the spine can elicit pain. The current study provides proof-of-concept feasibility that such a hypothesized imaging technique exists and is relatively simple.

Radiographic assessment alone, or in conjunction with other modalities, such as MRI in 2D slice planes with or without a dynamic component, is not adequate for characterizing the relative 3D architecture between the vertebral bodies, spinal cord, discs, and neural tissues and the change in this architecture during spinal motions. Indeed, it is this relationship, or change in overall relationships, that could lead to a transient neuropathology that may be responsible for pain. Architectural measurements such as those performed in the present study could potentially be useful for the identification of differences between symptomatic and asymptomatic subjects and could eventually predict potential sites/causes of future neuropathologic symptoms, leading to preventive treatment. However, because of the intra- and inter-subject variability, subject motion, small groups and large number of measurements, there was no evident pattern of statistical significance between the two groups. For instance, the standard deviations of the cord-to-canal distance and cord-to-canal offset measurements represented 21% and 49% of the respective average values for the asymptomatic subjects in the neutral position. Accordingly, and since it would be impossible or even meaningless to present the 210 raw measurements/calculations, only significant statistical differences were presented (Table 2). Also, the image processing procedures currently call for a significant amount of user interaction and time. Although such experiments could be conducted on larger groups and the image analysis could be automated to allow repeated measurements from different researchers, there is no guarantee that significant differences could be found between the two groups. Indeed, the large variation (7.3%) in the repeated measurement of the cord-to-canal relationship shows that measurement errors of small distances are amplified.

This approach and our investigation has other limitations as well. Notably, the sample size of the study is small, and the results provide only a preliminary demonstration of the general approach. Also, these and other linear measures were in absolute units and not normalized to take into account the variation in the size of the subjects. Lastly, the role of symmetry/asymmetry of the bilateral facet joints could potentially inform on architectural relationships, which was not measured here. Since tropism influences the relative kinematics of adjacent vertebrae [42,43], it likely influences the architectural relationships between neural and bone tissues during spine movements. Therefore, its measurement would help classify symptomatic patients and possibly to predict sites where transient nerve loading may occur.

Although the architectural measurements did not yield significant differences between the symptomatic and asymptomatic subjects with regards to the radiculopathy symptoms, 3D sMRI proved clinically beneficial. Indeed, we have demonstrated that a dynamic 3D imaging of the neural and bone elements of the cervical spine enables the identification of potential sites and/or causes of symptoms in symptomatic subjects without any conventional imaging evidence (Fig. 4). This outcome is most directly valuable to clinicians for the diagnosis and treatment options as demonstrated in the case study.

The case study that we present clearly illustrates how the stress MRI protocol was able to provide additional insight about the potential source of pain beyond the typical radiology report. In fact, the tissue deformation was obvious upon review of the images and did not require or necessitate even the architectural analysis (Fig. 4). Because of the individual's relatively young age, there was minimal spondylosis and no significant foraminal stenosis on the static MRI. This clinical scenario is relatively common – a history and physical exam consistent with cervical radiculopathy but no convincing MRI evidence of nerve root compression which leads to further studies including dynamic radiographic imaging, which are relatively insensitive, and EMG. When the EMG shows evidence of radiculopathy, the clinician is confronted with the possibility of performing surgery with relatively normal imaging. Stress MR imaging showing nerve root compression supported the neural tissue compression and provided support for surgical intervention based on imaging evidence. In fact, this imaging evidence also influenced the management of this symptomatic subject. Because of the positive imaging from the pain-provoking head position (Fig. 4), the site of a transient evoked nerve root compression was localized and that imaging was used to guide the clinician (A.H.) in his surgical intervention, which otherwise would have been unremarkable.

Although preliminary, these biomechanical and clinical results (Table 2; Fig. 4) demonstrate that the proposed approach may indeed have the sensitivity and precision to detect the 3D architectural relationships that may describe particular causes for the radiculopathy symptoms. The identified relevant architectural parameters (Table 2) may also provide guidance for future approaches to inform specific corrective procedures. This study suggests that through the use of 3D stress MRI it may be possible to localize a discrete source of neural compression, which is demonstrable only in the specific painful "stressed" position. Anatomic and active "targeting" of the source of the patient's pain may result in more rapid identification and more accurate treatment of the patient's pathology. Indeed, this was the case for at least one symptomatic subject in the present study (Fig. 4), suggesting that such an approach to imaging pain may be helpful. This may reduce the medical costs associated with failed or prolonged treatment, and the time lost from work. Also 3D sMRI may provide much needed insight into the biomechanical relationships between tissues in the spine in normal and diseased states.

Conflict of interest statement

None of the authors have any financial or personal relationships to disclose related to this study.

Acknowledgements

This project was supported by grant support from the Cervical Spine Research Society and the Catherine Sharpe Foundation.

References

[1] Peng B, Wu W, Hour S, Li P, Zhang C, Yang Y. The pathogenesis of discogenic low back pain. J Bone Joint Surg Br 2005;87(1):62–7.
[2] Scutellari PN, Rizzati R, Antinolfi G, Malfaccini F, Leprotti S, Campanati P. The value of computed tomography in the diagnosis of low back pain. A review of 2012 cases. Minerva Med 2005;96(1):41–59.
[3] Nuckley DJ, Konodi MA, Raynak GC, Ching RP, Chapman JR, Mirza SK. Neural space integrity of the lower cervical spine: effect of anterior lesions. Spine 2004;29(6):642–9.
[4] Nuckley DJ, Konodi MA, Raynak GC, Ching RP, Mirza SK. Neural space integrity of the lower cervical spine. Effect of normal range of motion. Spine 2002;27(6):587–95.
[5] Hollingworth W, Dixon AK, Todd CJ, et al. Self reported health status and magnetic resonance imaging findings in patients with low back pain. Eur Spine J 1998;7(5):369–75.
[6] Onan OA, Heggeness MH, Hipp JA. A motion analysis of the cervical facet joint. Spine 1998;23(4):430–9.
[7] Bogduk N, Mercer S. Biomechanics of the cervical spine. I: normal kinematics. Clin Biomech 2000;15(9):633–48.
[8] Winkelstein BA, Myers BS. Experimental and computational characterization of three dimensional cervical spine flexibility. Stapp Car Crash J 2000;44:139–58.
[9] Panjabi MM, Crisco JJ, Vasavada A, Oda T, Cholewicki J, Nibu K, et al. Mechanical properties of the human cervical spine as shown by three-dimensional load displacement curves. Spine 2001;26(24):2692–700.
[10] Levitz CL, Reilly PJ, Torg JS. The pathomechanics of chronic, recurrent cervical nerve root neuropraxia. Am J Sports Med 1997;25(1):73–6.
[11] Meyer SA, Schulte KR, Callaghan JJ, et al. Cervical spinal stenosis and stingers in collegiate football players. Am J Sports Med 1994;22(2):158–66.
[12] Brown T, Reitman CA, Nguyen L, Hipp JA. Intervertebral motion after incremental damage to the posterior structures of the cervical spine. Spine 2005;30(17):503–8.
[13] Kandziora F, Pflugmacher R, Scholz M, et al. Comparison between sheep and human cervical spines: an anatomic, radiographic, bone mineral density, and biomechanical study. Spine 2001;26(9):2640–1.
[14] Kaneoka K, Ono K, Inami S, Hayashi K. Motion analysis of cervical vertebrae during whiplash loading. Spine 1999;24(8):763–9.
[15] Van de Kelft E, van Vyve M. Diagnostic imaging algorithm for cervical soft disc herniation. Acta Chir Belg 1995;95(3):152–6.
[16] Strobel K, Pfirrmann CW, Schmid M, Hodler J, Boos N, Zanetti M. Cervical nerve root blocks: indications and role of MR imaging. Radiology 2004;233(1):87–92.
[17] Sohn HM, You JW, Lee JY. The relationship between disc degeneration and morphologic changes in the intervertebral foramen of the cervical spine: a cadaveric MRI and CT study. J Korean Med Sci 2004;19(1):101–6.
[18] Czervionke LF, Daniels DL, Ho PSP, et al. Cervical neural foramina: correlative anatomic and MR imaging study. Neuroradiology 1988;169(3):753–9.
[19] Karhu JO, Parkkola RK, Komu ME, Kormano MJ, Koskinen SK. Kinematic magnetic imaging of the upper cervical spine using a novel positioning device. Spine 1999;24(19):2046–56.
[20] Kimura S, Hesselink JR, Garfin SR, Kawaji Y, Hasegawa K, Hargens AR. Axial load-dependent cervical spinal alterations during simulated upright posture: a comparison of healthy controls and patients with cervical degenerative disease. J Neurosurg Spine 2005;2(2):137–44.
[21] Simon S, Davis M, Odhner D, Udupa JK, Winkelstein B. CT imaging techniques for describing motions of the cervicothoracic junction and cervical spine during flexion, extension, and cervical traction. Spine 2006;31(1):44–50.
[22] Winkelstein BA, Myers BS. Importance of nonlinear and multivariable flexibility coefficients in the prediction of human cervical spine motion. J Biomech Eng 2002;124(5):504–11.
[23] Panjabi MM, Brand RA, White AA. Three-dimensional flexibility and stiffness properties of the human thoracic spine. J Biomech 1976;9(4):155–82.
[24] Panjabi MM, Crisco JJ, Vasavada A, et al. Mechanical properties of the human cervical spine as shown by three-dimensional load-displacement curves. Spine 2001;26(24):2692–700.
[25] Brunner P, Ernst RR. Sensitivity and performance time in NMR imaging. J Magn Reson 1979;33:83–106.
[26] Ishii T, Mukai Y, Hosono N, et al. Kinematics of the upper cervical spine in rotation: in vivo three-dimensional analysis. Spine 2004;29(7):E139–44.
[27] Ishii T, Mukai Y, Hosono N, et al. Kinematics of the subaxial cervical spine in rotation in vivo three-dimensional analysis. Spine 2004;29(24):2826–31.
[28] Ishii T, Mukai Y, Hosono N, et al. Kinematics of the cervical spine in lateral bending in vivo three-dimensional analysis. Spine 2006;31(2):155–60.
[29] Udupa JK, Hirsch BE, Hillstrom HJ, Bauer GR, Kneeland JB. Analysis of in vivo 3-D internal kinematics of the joints of the foot. IEEE Trans Biomed Eng 1998;45(11):1387–96.
[30] Siegler S, Udupa JK, Ringleb SI, et al. Mechanics of the ankle and subtalar joints revealed through a 3D quasi-static stress MRI technique. J Biomech 2005;38(3):567–78.
[31] Ringleb SI, Udupa JK, Siegler S, et al. The effect of ankle ligament damage and surgical reconstructions on the mechanics of the ankle and subtalar joints revealed by three-dimensional stress MRI. J Orthop Res 2005;23(4):743–9.
[32] Liu J, Udupa JK, Saha PK, et al. Rigid model-based 3D segmentation of the bones of joints in MR and CT images for motion analysis. Med Phys 2008;35(8):3637–49.
[33] Liu J, Udupa JK. Oriented active shape models. IEEE Trans Med Imaging 2009;28(4):571–84.
[34] Udupa JK, Odhner D, Samarasekera S, et al. 3DVIEWNIX: an open, transportable, multidimensional, multimodality, multiparametric imaging software system. SPIE Proc 1993;2164:58–73.
[35] Madabhushi A, Udupa JK, Souza A. Generalized scale: theory, algorithms, and application to image inhomogeneity correction. Comp Vis Imag Understanding 2006;101:100–21.
[36] Nyul LG, Udupa JK, Zhang X. On standardizing the MR image intensity scale. Mag Res Med 1999;42:1072–81.
[37] Maes F, Collignon A, Vandermeulen D, Marchal G, Suetens P. Multimodality image registration by maximization of mutual information. IEEE Trans Med Imaging 1997;16(2):187–98.
[38] Falcao A, Udupa JK, Samarasekera S, Sharma S, Hirsch BE, Lotufo R. User-steered image segmentation paradigms: live wire and live lane. Graph Mod Image Proc 1998;60:233–60.
[39] Udupa JK, Samarasekera S. Fuzzy connectedness and object definition: theory, algorithms, and applications in image segmentation. Graph Mod Image Proc 1996;1996(58):246–61.
[40] Muhle C, Bischoff L, Weiner D, et al. Exacerbated pain in cervical radiculopathy at axial rotation, flexion, extension and coupled motion of the cervical spine. Invest Radiol 1998;33(5):279–88.
[41] Gemici C. Lhermitte's sign: review with special emphasis in oncology practice. Crit Rev Oncol Hematol 2010;74(2):79–86.
[42] Cyron BM, Hutton WC. Articular tropism and stability of the lumbar spine. Spine 1980;5(2):168–72.
[43] Masharawi Y, Rothschild B, Salame K, Dar G, Peleg S, Hershkovitz I. Facet tropism and interfacet shape in the thoracolumbar vertebrae: characterization and biomechanical interpretation. Spine 2005;30(11):E281–92.